Geophysical Journal International

Geophys. J. Int. (2010) **181,** 985–996 doi: 10.1111/j.1365-246X.2010.04550.x

Detecting seasonal variations in seismic velocities within Los Angeles basin from correlations of ambient seismic noise

Ueli Meier,* Nikolai M. Shapiro and Florent Brenguier

Institut de Physique du Globe de Paris, Equipe de Sismologie 4 *Place Jussieu Case* 89, 75252 *Paris cedex* 05, *France. E-mail: meierue@ipgp.jussieu.fr*

Accepted 2010 February 2. Received 2010 January 14; in original form 2009 May 11

SUMMARY

We analyse 3 yr of continuous seismic records from broad-band stations of the Caltech Regional Seismic Network (CI) in vicinity of the Los Angeles basin. Using correlations of ambient seismic noise, relative velocity variations in the order of 0.1 per cent can be measured between all interstation pairs. It is the first time that such an extensive study between 861 interstation pairs over such a large area has been carried out. We perform these measurements using the 'stretching' technique, assuming that one of the two waveforms is merely a stretched version of the other. Obviously this assumption is always violated and the two waveforms are generally decorrelated due to temporal changes in the Earth crust, due to different sources or simply because the cross-correlations are not fully converged. We investigate the stability of these measurements by repeating each measurement over various time-windows of equal length. On average between all interstation pairs in the Los Angeles basin a seasonal signal in the relative velocity variation is observed, with peaks and troughs during winter and summer time, respectively. Generally the observed signal decreases with increasing interstation distance and relative traveltime perturbations can only be measured up to an interstation distance of 60 km. Furthermore, the traveltime perturbations do not depend on azimuth of station pairs, suggesting that they are not related to seasonal variations of the noise sources. Performing a simple regionalization by laterally averaging measurements over a subset of stations we found the sedimentary basin showing the most consistent signal and conclude that the observed seasonality might be induced either by changes in the ground-water aquifer or thermo-elastic strain variations that persist down to a depth of 15–22 km.

Key words: Interferometry; Coda waves; Crustal structure.

1 INTRODUCTION

It has become common ground in seismology that the cross-correlation of a random wave field sensed at two different seismic stations yields the Green's function between the two stations (e.g. Weaver & Lobkis 2001; Larose *et al.* 2006; Gouédard *et al.* 2008). An immediate consequence of this theorem, is that any seismic instrument can be used as a potential source, resulting in increased lateral resolution compared to conventional active seismic imaging. It has been demonstrated that surface wave Green's functions can be extracted by cross-correlation of multiply scattered seismic coda (Campillo & Paul 2003), as well as by cross-correlation of ambient seismic noise (Shapiro & Campillo 2004; Sabra *et al.* 2005a,b; Shapiro *et al.* 2005). This new data source has been exploited extensively to perform conventional surface wave dispersion measurements on local and regional scale (e.g. Brenguier *et al.* 2007; Lin *et al.* 2007; Moschetti *et al.* 2007; Stehly *et al.* 2009).

In all of these studies the surface waves were retrieved from continuous ambient seismic noise records of a given duration and treated as being stationary. Green's functions retrieved from ambient seismic noise records over different time periods are strictly speaking not stationary, and the temporal variations contain useful information. Exploring these temporal variations, it is for example possible to detect instrumental errors (Stehly *et al.* 2007; Sens-Schönfelder 2008) or to estimate slight changes in the seismic velocity structure. Temporal variations of the media seismic velocity are generally too small to be detected by direct waves. The longer the waves travel through the medium the more sensitive they become to velocity variations. Later arriving phases, generally attributed to multiply scattered waves, are therefore of great potential to detect relative temporal variations in the subsurface. Estimating relative changes in the mean shear wave velocity from comparison of multiply scattered coda waves dates back to Poupinet *et al.* (1984), who measured temporal variations of crustal velocities from seismograms recorded from a pair of micro-earthquakes occurring

*Now at: Dalle Molle Institute for Artificial Intelligence (USI/SUPSI/IDSIA) Galleria 2, 6928 Manno-Lugano, Switzerland.

at different dates with nearly identical hypocentre and magnitude. Such events are however very rare, which explains the limited applicability of this technique. Experiments with repeated active seismic sources are also a possibility to obtain similar waveforms but are in general rather expensive (e.g. Nishimura *et al.* 2000; Wegler *et al.* 2006). In contrast, continuous ambient seismic noise records from permanent or semi-permanent networks are more cost effective and furthermore the position of the receivers and hence the apparent sources does not change with time. Sens-Schönfelder & Wegler (2006) demonstrated that Green's functions retrieved from ambient seismic noise records contain multiply scattered waves, which can be analysed to monitor small temporal variations of the subsurface. Indeed, this technique has been successfully applied to detect small velocity variations in volcanoes (e.g. Sens-Schönfelder & Wegler 2006). Similarly, Wegler & Sens-Schönfelder (2007) and Brenguier *et al.* (2008b) detected a decrease of relative seismic velocities that coincidence with the occurrence of an earthquake and Brenguier *et al.* (2008a) detected a decrease in relative velocity prior to volcanic eruptions. The same principle has also been successfully applied in laboratory experiments with active sources to detect small variations in the medium of interest (e.g. Snieder *et al.* 2002; Grêt *et al.* 2006; Leroy & Derode 2008; Hadziioannou *et al.* 2009; Larose & Hall 2009).

In this paper, we extend this technique to broad-band data from the Caltech Regional Network (CI) and analyse 3 yr of continuous seismic records from 42 broad-band stations. It is for the first time that such an extensive study, analysing relative velocity changes from 861 interstation pairs covering an area of approximately 90 × 190 km, has been carried out. We measured relative traveltime perturbations between all the interstation pairs in various frequency bands between 0.1 and 2 Hz in the Los Angeles basin. We mainly opted for this frequency band because it includes the microseismic peak (Stehly *et al.* 2006). We perform repeated measurements over various time-windows and computed corresponding uncertainties from the variance of those repeated measurements. In principle these uncertainties should depend on the amount of decorrelation as described by the correlation coefficient, central frequency, bandwidth and length of the time window over which the measurements are performed (Hadziioannou *et al.* 2009; Weaver, private communication, 2010). Our uncertainty estimates do however not depend on the maximum correlation coefficient and we therefore decided to discard measurements from two waveforms whose maximum correlation coefficient after stretching is below a certain threshold. In this way we simply discard bad quality measurements from further analysis. Using a simple regionalization scheme, laterally averaging measurements from a subset of stations, we were able to identify the sedimentary basin as having the most consistent signal. These are however still preliminary and qualitative results. In order to further improve on these results and quantitatively map relative velocity changes in the Earth's crust on regional scale a better understanding of the spatial sensitivities of these measurements is required. A problem that to the best of our knowledge is still an open issue.

2 DATA

We analysed 3 yr of continuous seismic records from 42 broad-band stations of the Caltech Regional Network (CI) in the vicinity of the Los Angeles basin (Fig. 1). Not only are we using many more stations than in previous studies but also cover a much bigger area with a maximum interstation distance of ≈190 km parallel to the coast (DGR-MOP) and ≈90 km perpendicular to the coast (BFS-RPV). The data were obtained from the Southern California Earthquake Data Center (SCEDC). We only analysed the vertical component and performed standard data processing: (1) removed the instrument response, (2) down-sampled the data to a sampling rate of 0.05 s, (3) performed spectral whitening in the frequency band of 0.0064–4 Hz, (4) applied one-bit normalization and

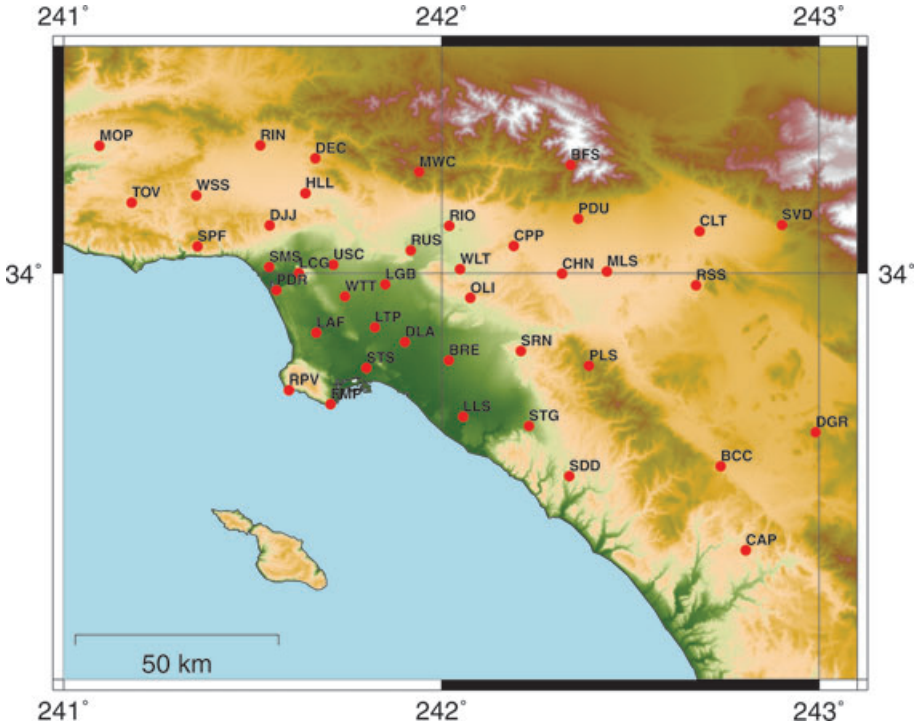

Figure 1. 42 broad-band stations indicated by the red circles of the Caltech Regional Network (CI) considered in this study.

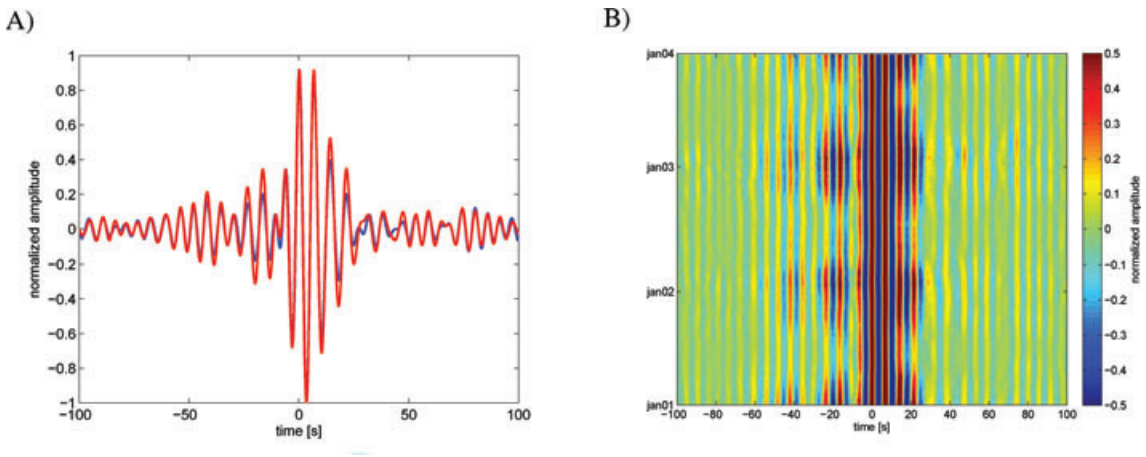

Figure 2. (a) Sixty-day stacked cross-correlation function starting at 2001 May 1 (blue) together with the 3-yr reference stack (red) for station-pair DEC-USC. (b) All 60-d stacks over the 3-yr period for station-pair DEC-USC. The cross-correlations are filtered between 0.1 and 0.2 Hz.

(5) computed 1-d cross-correlations for all the 861 interstation pairs and 42 autocorrelations for a time-lag of ±600 s. Stacking the 1 d correlations over the whole 3-yr time period results in the reference stack. In order to measure the temporal evolution of relative travel-time perturbations with respect to the reference stack, we computed 60 d-long stacks over the whole 3 yr period in a 5 d moving window. In Fig. 2, a 60-d stack together with the reference stack is shown for the station-pair DEC-USC (a), as well as all 60-d stacks over the whole 3-yr period for the same station-pair (b). Note that slight changes in coherent phases arriving after ±25 s over the 3-yr period are already visible. Furthermore, seasonal variations in amplitudes of the 60-d stacks are also visible.

3 MEASURING RELATIVE VELOCITY PERTURBATIONS

By measuring relative velocity perturbations ($\delta v/v$) from the coda of two similar waveforms it is generally assumed that $\delta v/v$ is spatially homogeneous. This implies that the relative time-shift ($\delta\tau/\tau$) between the two waveforms is independent of the lapse time (τ) at which it is measured and $\delta v/v = -\delta\tau/\tau = \text{const}$. (Snieder *et al.* 2002). In principle it would be sufficient to measure $\delta\tau$ at one particular lapse time τ to estimate $\delta\tau/\tau$. Mainly because the relative velocity perturbations are only approximately homogeneous but also due to uncertainties in measuring $\delta\tau$ a statistical approach is generally chosen and $\delta\tau_i$ is measured at various lapse times τ_i.

There are two similar techniques to measure $\delta\tau_i$ within time windows of length T centred around τ_i. Snieder *et al.* (2002) estimated $\delta\tau_i$ as the time-shift corresponding to the maximum of the cross-correlation of the two waveforms in each window of length T centred around τ_i. $\delta\tau/\tau$ is then approximated as the mean of all $\delta\tau_i/\tau_i$ measured over a window of length L, where $L > T$. Another technique estimates $\delta\tau_i$ from the phase of the cross-spectrum of the two waveforms in each window of length T centred around τ_i. The time-shift $\delta\tau_i$ is then obtained by fitting a line, starting at the origin, to the phase of the cross-spectrum $\phi(f) = 2\pi\delta\tau_i f$ (Poupinet *et al.* 1984). With this technique the accuracy of the individual measurements is not limited by the sampling rate. $\delta\tau/\tau$ and hence $\delta v/v$ is then obtained by a linear regression of the various $\delta\tau_i$ measurements over a window of length L, where $L > T$. Both techniques require the choice of an appropriate value for the window length T, which should be long enough to obtain meaningful correlations or cross-spectra but also short enough to ensure that the distortion of the two waveforms is small within these windows. Sens-Schönfelder & Wegler (2006) proposed instead to estimate $\delta\tau/\tau$ as the factor by which the time axis on one waveform has to be stretched or compressed to obtain the best correlation with the other waveform over the time-window of length L. An obvious advantage to the above mentioned technique, is that there is no need to set an appropriate value for T and more importantly, a direct estimate of $\delta\tau/\tau$ is obtained. In a recent study Hadziioannou *et al.* (2009) discussed advantages and drawbacks of both above mentioned techniques.

3.1 Uniform scaling of the time axis (Stretching)

More formally, let's assume we have two waveforms, a reference waveform $f^{\text{ref}}(t)$ and a current waveform $f^{\text{cur}}(t)$. A stretched version of $f^{\text{cur}}(t)$ is defined as

$$f_\epsilon^{\text{cur}}(t) = f^{\text{cur}}[t(1+\epsilon)], \tag{1}$$

where ϵ is the stretching coefficient. We then look for ϵ that maximizes:

$$C(\epsilon) = \frac{\int f_\epsilon^{\text{cur}}(t) f^{\text{ref}}(t)\mathrm{d}t}{\sqrt{[\int f_\epsilon^{\text{cur}}(t)^2\mathrm{d}t][\int f^{\text{ref}}(t)^2\mathrm{d}t]}}, \tag{2}$$

where integration is over a specific time window $t_1 \le t \le t_2$ of length $L = t_2 - t_1$ and the relative time-shift of f^{cur} with respect to f^{ref} is simply given by: $\delta\tau/\tau = -\epsilon_{\max}$.

If f^{cur} is a stretched version of f^{ref}, we will find $C_{\max} = 1$ at some $\epsilon_{\max} \neq 0$. In general the two waveforms f^{cur} and f^{ref} will slightly differ due to temporal variations in the Earth crust, due to different sources or because the correlations are not fully converged (i.e. $C_{\max} < 1$). Strong distortion and weak stretching might furthermore indicate a change of structure rather than a global velocity change. In other words, the assumptions on which eq. (2) is based are always going to be violated, leading to errors in the estimation of $\epsilon_{\max}$. It is therefore crucial to investigate the stability of the measurements as well as to try to come up with uncertainty estimates that serve as a measure of how reliable a particular measurement is. So far it has been shown that increasing the window length L and/or the bandwidth can reduce the effect of differing waveforms (Hadziioannou *et al.* 2009). It is however still an unresolved issue how slightly differing waveforms are affecting the estimation of the stretching coefficient (Weaver, private communication, 2010).

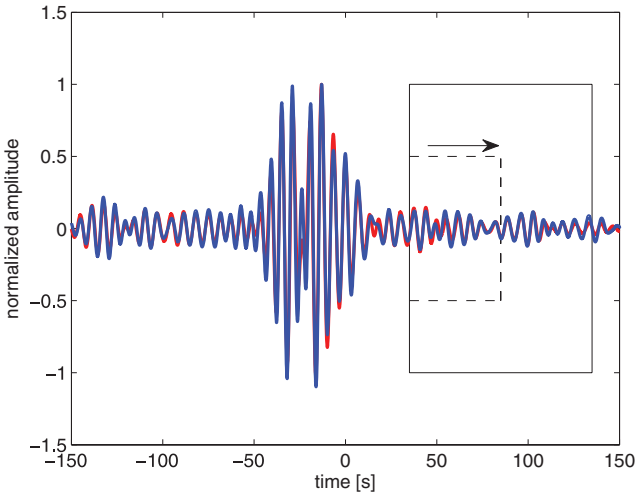

Figure 3. Sixty-day stacked cross-correlation function filtered between 0.1 and 0.2 Hz starting at 2001 May 1 (blue) together with the 3-yr reference stack (red) for station-pair BRE-CHN. The time window of length $L = 10T_{\max}$ (black box) and the time window of length $L = 5T_{\max}$ (black dashed box) that is shifted towards the right-hand side and over which the relative time-shifts are measured repeatedly is also shown for positive lapse times.

Here we take a pragmatic approach in order to investigate the stability of the performed measurements and perform repeated measurements in shifted but overlapping time-windows of equal length. If one of the two waveforms is merely a stretched version of the other, all repeated measurements should yield identical results. The variance of the repeated measurements can therefore be seen as an error estimate of the $\delta\tau/\tau$ measurements. In addition, we also keep track of the maximum value of the correlation coefficient and discard measurements whose best stretching coefficient results in a correlation coefficient below a certain threshold. In this way measurements from waveforms that differ too much are simply excluded.

In order to measure relative time-shifts in the coda of a 60-d stack with respect to the reference stack an appropriate time window has to be chosen. We computed cross-correlations for a time-lag of ± 600 s. In order to obtain meaningful measurements of $\delta\tau/\tau$ this is obviously too long and since we are interested in comparing measurements for different interstation distances up to 189 km, an adaptive starting time (t_1) of the time window has to be chosen. Since we are not interested in direct surface waves, we set for all interstation pairs the starting time $t_1 = d_i/v_{\min}$, where d_i is the ith interstation pair distance and $v_{\min} = 1\ \mathrm{km\,s^{-1}}$ is the minimum apparent velocity. In order to adapt the window length to different frequency ranges the time window length is set to $L = 10T_{\max}$, where $T_{\max}$ is the maximum period of the considered bandwidth. We then repeat the measurement k times in a smaller time window of length $L = 5T_{\max}$ and increased starting time $t_{\text{start}} = t_1 + (k-1)T_{\max}$, where $k = 1, .., 5$ (Fig. 3). From the five measurements in smaller time windows we compute error estimates of $\epsilon_{\max}$ around the values estimated from the measurement performed over the long time window.

In Fig. 4, the cross-correlation as a function of the stretching coefficient (eq. 2) is shown for a 60-d stack starting at 2001 May 1 with respect to the 3-yr reference stack for station-pair BRE-CHN in the negative (A, C) and positive (B, D) time windows, respectively. The dashed lines are computed in overlapping time-windows of length $L = 50s$ with starting times $t_1 = \pm 35, \pm 45, .., \pm 85s$, and the solid line is computed over a time window of length $L = 100$ s starting at $t_1 = \pm 35$. A zoom around the maximum is shown in (C) and (D) with the stretching coefficient that maximizes eq. (2) (red, solid), and the uncertainties (red, dashed) given by the standard deviation of the repeated measurements over the shorter time windows (dashed curves). The value of the correlation coefficient gives a measure of how well the two waveforms match after stretching, and we would intuitively guess that the lower the maximum correlation coefficient the lower the quality of the measurements. In Section 4, we will demonstrate how only considering measurements with a correlation coefficient bigger than a certain threshold increases the quality of the result.

In this example we evaluated $C(\epsilon)$ for stretching coefficients ranging from $[-0.1 : 0.1]$ with an increment of $\Delta\epsilon = 10^{-4}$, the resulting $\epsilon_{\max}$ has therefore an accuracy of 10^{-4} and 2001 evaluations of $C(\epsilon)$ are required to find the maximum. This is obviously far from being efficient and considering that we ultimately perform 207 measurements for 861 interstation pairs in positive and negative time windows a more efficient algorithm to maximize $C(\epsilon)$ is required. We opted for a line search algorithm (Nabney 2002) that allows us to estimate $C_{\max}$ with an accuracy of 10^{-4} requiring much less evaluations of $C(\epsilon)$. The increased efficiency came however at the price, that we risk to find only a local maximum. It is therefore crucial to chose appropriate initial bounds on ϵ. If the initial search bound is too broad, there are likely to be various maxima in the correlation coefficient function $C(\epsilon)$, if the initial search bound is however too narrow, there might be no maximum at all and our results might be biased. In other words, the initial search bound reflects the maximum traveltime perturbations between a 60-d and the reference stack we are expecting *a priori*. After evaluating and plotting $C(\epsilon)$ for various interstation pairs in the different frequency bands considered, we set the initial search range to $-0.01 \leq \epsilon \leq 0.01$ for the frequency ranges 0.1–0.2, 0.1–1 and 0.1–2 Hz and to $-0.005 \leq \epsilon \leq 0.005$ for the frequency range 0.5–2 Hz, respectively.

4 RESULTS

We measured $\delta\tau/\tau$ from all the 207, 60-d stacks with respect to the reference stack for all 861 interstation pairs in a particular time window of length L starting at $\pm t_1$. Note that for each cross-correlation the two measurements for positive and negative lapse times are treated as two independent measurements. In addition, we computed the corresponding standard deviations as the variance of the repeated measurements. In total we performed $6 \times 178\,227$ measurements in positive and negative time windows. Performing that many measurements requires an automated quality control of the 60-d stacked cross-correlations. There are various problems that might arise, limited data availability during some days, missing information about the instrument response on other days, or unknown instrumental time-shifts for some stations, just to name a few. If one of the above mentioned problems arose during a particular time-period, the resulting 60-d stacks are likely to be corrupted. In order to detect those spurious correlations we first check if the two waveforms are correctly aligned and only perform measurements if the maximum of the cross-correlation in the considered time window occurs at time lags smaller than ± 5 times the sampling rate. In this way we reject spurious waveforms that for one reason or another are not suitable to perform the measurements and ultimately would degrade the results. For illustrative purposes we start presenting our results with a comparison from one particular interstation pair in various frequency bands.

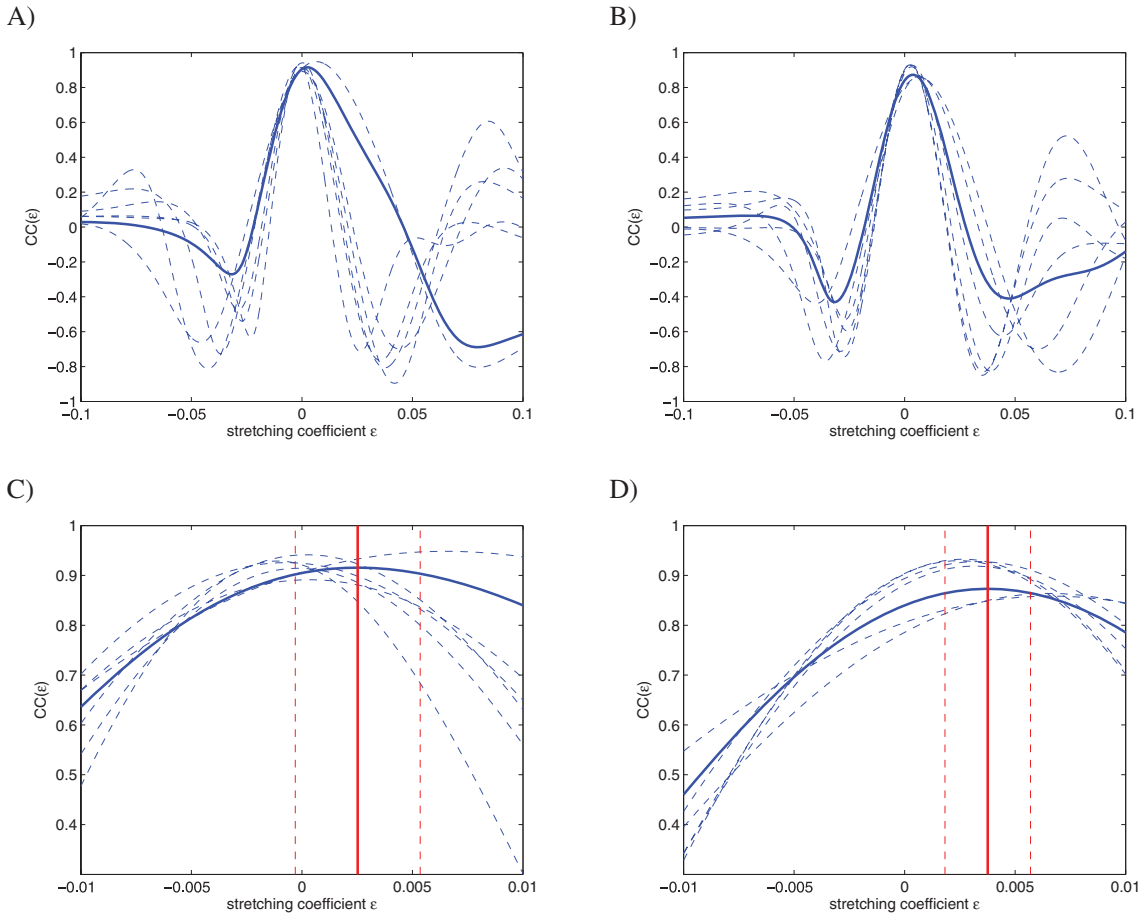

Figure 4. Correlation coefficient as a function of the stretching coefficient (eq. 2) computed over 100 s long (solid) and 50 s long (dashed) windows for the two waveforms shown in Fig. 3 for negative (a, c) and positive (b, d) lapse times. Panels (c) and (d) show a zoom around the maximum of the cross correlation function of the 100s long (blue, solid) window together with the maximum (red, solid) ± 1 *SD* (red, dashed), estimated from the five repeated measurements over 50 s long (blue, dashed) windows. Note the different horizontal scale in (c) and (d).

4.1 Comparison of $\delta\tau/\tau$ for BRE-CHN, in four different frequency ranges: 0.1–0.2, 0.1–1 0.1–2 and 0.5–2 Hz

We measured $\delta\tau/\tau$ from 207, 60-d stacks with respect to the reference stack for the interstation pair BRE-CHN and compare the obtained results from cross-correlations filtered between 0.1–0.2, 0.1–1, 0.1–2 and 0.5–2 Hz. In Fig. 5, the outcome of this comparison is summarized: $\delta\tau/\tau$ measurements are shown together with the corresponding standard deviations in the positive (blue) and negative (red) time window (left-hand column); the corresponding $C_{\max}$ values are shown for positive (blue) and negative (red) time windows (middle column); and all the 207, 60-d stacks in the considered time windows are shown (right-hand column). From top to bottom the corresponding cross-correlations where filtered between 0.1–0.2 (a–c), 0.1–1 (d–f), 0.1–2 (g–i) and 0.5–2 Hz (j–l). Note how the uncertainties on the measurements decrease with increasing bandwidth. Low $C_{\max}$ values are an indication that the 60-d stack is not merely a stretched/compressed version of the reference stack, and that the two waveforms are highly decorrelated. In this case the corresponding estimates of $\delta\tau/\tau$ are obviously less precise and ultimately meaningless. This observation is most evident in the frequency range between 0.5 and 2 Hz, where the $C_{\max}$ values in the positive time window (K, blue) are very low. Looking at the waveforms (L, right-hand panel) this is not surprising because there are no coherent phases in this frequency range. Since the interstation pair BRE-CHN is perpendicular to the coast, the positive time window corresponds to waves traveling towards the ocean, a direction which is known to have very weak noise sources. The same observation can be made for the other three frequency ranges, but to a lesser extent. Furthermore, it is worth noting that $\delta\tau/\tau$ in the positive and negative time windows show a seasonal variation with peaks and troughs during winter and summer time, respectively. The amplitude of this variations is in the order of ± 0.5 per cent in the frequency range between 0.1 and 0.2 Hz (a) and in the order of ± 0.2 per cent in the frequency ranges 0.1–1 Hz (d) and 0.5–2 Hz (g), respectively.

4.2 Laterally averaged distribution of $\delta\tau/\tau$ for all 861 interstation pairs

In a next step we computed averages and standard deviations of $\delta\tau/\tau$ from all the 861 interstation pairs. We assume that measurements at particular time steps are following a Gaussian distribution with mean and standard deviation computed as described in Section (3.1). We then plot the resulting Gaussian probability density function (pdf) for each time step over the whole 3-yr period (Fig. 6), merely for illustrative purposes. Fig. 6 can be seen as a summary of

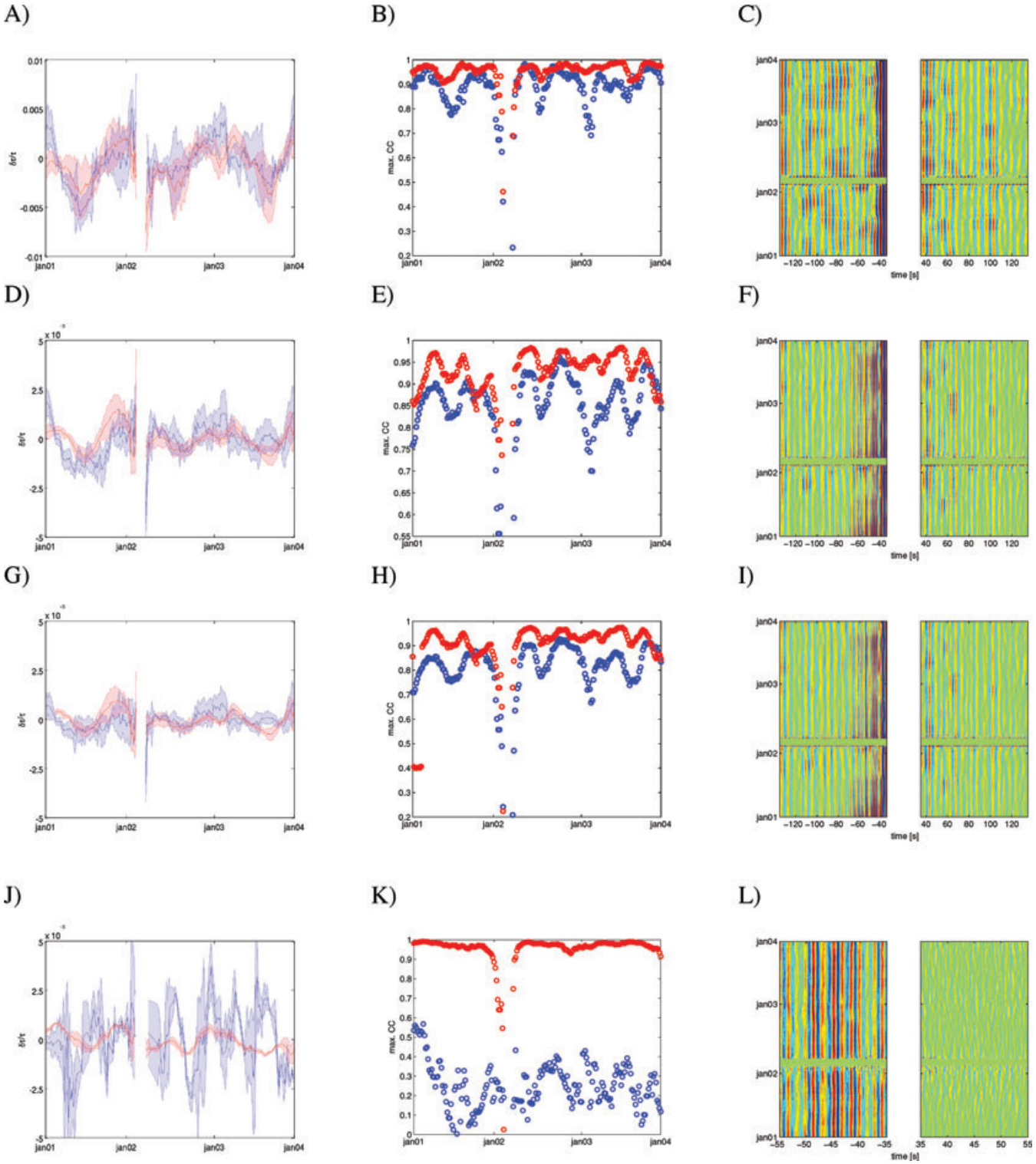

Figure 5. (a) Relative time-shift measurements (solid) ± 1 *SD* (shaded) of all 207, 60-d stacks with respect to the reference stack, measured in the positive (blue) and negative (red) time window ($L = 100$ s) for the interstation pair BRE-CHN in the frequency range between 0.1 and 0.2 Hz. (b) Values of the maximum correlation coefficient $C_{\max}$ in the positive (blue) and negative (red) time window. (c) All the 207, 60-d stacks filtered between 0.1 and 0.2 Hz, only the time windows over which the measurements were performed are shown. (d–f) Similar plots as (a–c) only that the cross-correlations are filtered between 0.1 and 1 Hz. (g–i) Similar plots as (a–c) only that the cross-correlations are filtered between 0.1 and 2 Hz. (j–l) Similar plots as (a–c) only that the cross-correlations are filtered between 0.5 and 2 Hz, note the shorter window length of $L = 50$ s. Vertical axes are changing in left-hand and middle columns.

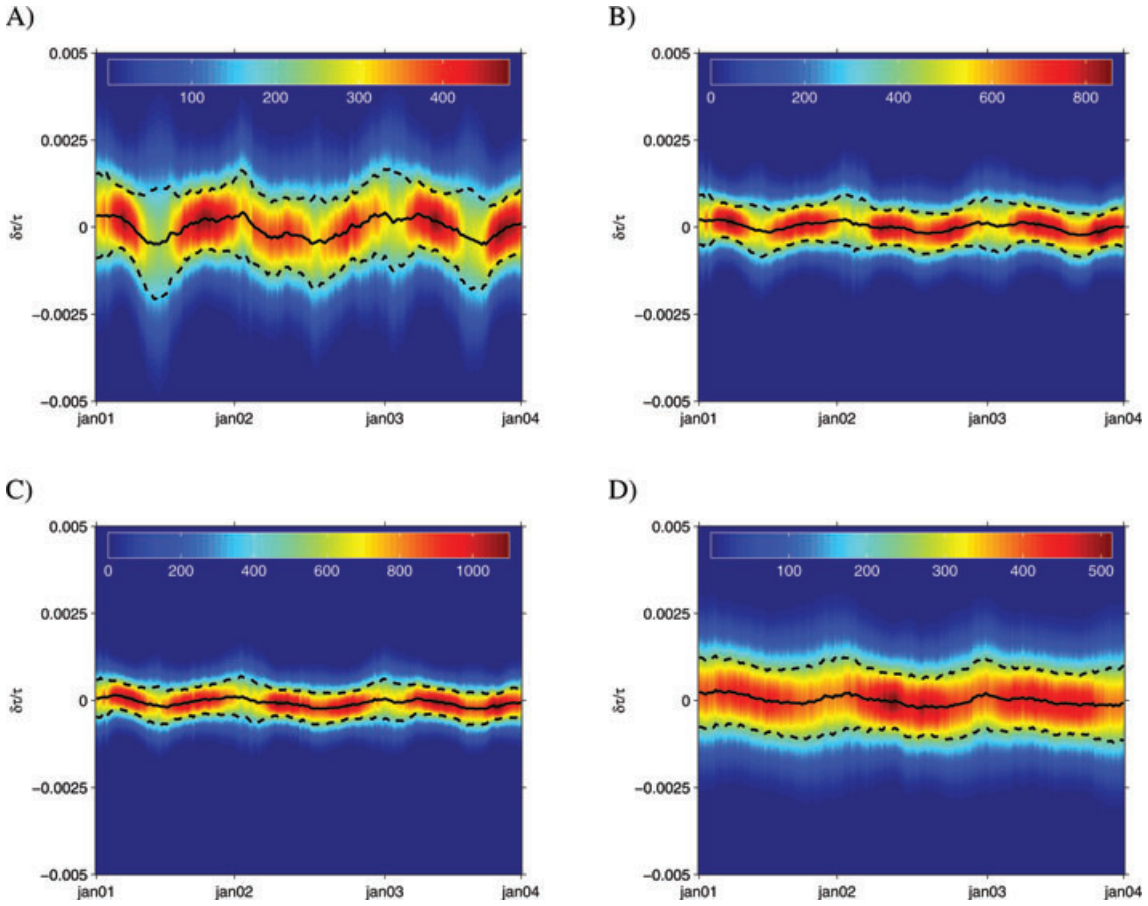

Figure 6. Gaussian pdfs of $\delta\tau/\tau$ with superimposed mean (black) ± 1 *SD* (dashed) for all 861 interstation pairs over a 3 yr period in various frequency bands, 0.1–0.2 (a), 0.1–1 (b),0.1–2 (c) and 0.5–2 Hz (d).

all the performed measurements. The mean (black) shows a clear seasonal variation. Note however that standard deviations (dashed) are rather big especially for the frequency range between 0.1 and 0.2 Hz (Fig. 6a). This might be due to the fact that we averaged measurements over various interstation pair distances, ranging from 6 to 190 km, various azimuths of station pairs and considered all paths that correspond to varying geological regimes. The more likely reason for this high standard deviations is however the small bandwidth that makes the measurements less stable to distortions of the waveforms (Hadziioannou *et al.* 2009). And indeed as can be seen for the other frequency bands the broader the bandwidth the more stable the measurements are. Another problem is that we considered all the measurements, some of these measurements are potentially from waveforms that differ too much even after stretching. Consequently, the maximum correlation coefficient of those measurements is low and indeed if all measurements with $C_{\max} < 0.9$ are excluded the resulting standard deviation of the distribution of $\delta\tau/\tau$ is much smaller (Fig. 7). We conclude that seasonal variations of $\delta\tau/\tau$ measurements with peaks and troughs during winter and summer time, respectively, are a robust feature in the studied area and that in order to obtain more robust results the bandwidth can be increased. Furthermore, it is crucial to exclude measurements from waveforms that differ too much as described by $C_{\max}$. In what follows we will focus further discussion of the results on the seasonal variations and will only consider measurements performed over the frequency range 0.1–2 Hz.

4.3 Relative time-shifts as a function of interstation pair distance

In order to further investigate the origin of the observed signal we decided to investigate the dependence of $\delta\tau/\tau$ with respect to interstation pair distance. In Fig. 8, the distribution of the average is plotted for six different interstation pair distances, 0–20 (top, left-hand panel), 20–40 (top, middle panel), 40–60 (top, right-hand panel), 60–80 (bottom, left-hand panel), 80–100 (bottom, middle panel) and for interstation pair distances $>$100 km (bottom, right-hand panel). Note that between 40 and 60 km the signal becomes weaker and finally disappears completely. This suggests that in the frequency range considered (0.1–2 Hz), seasonal variations in $\delta\tau/\tau$ can only be observed for interstation pair distances up to 40–60 km. A possible explanation for this observation might be, that less coherent phases are present in the considered time-windows for long interstation pair distances due to attenuation. Looking at the histogram of the maximum correlation coefficient as a function of interstation pair distance (Fig. 9) it is nicely visible that the bigger the interstation-pair distance the smaller the corresponding maximum correlation coefficients of the stretched waveforms become. For long interstation pair distances stacking only 60-d of ambient seismic noise records is probably not long enough. Consequently the 60-d stack didn't fully converge and differ too much with respect to the 3-yr-long reference stack. This suggests that if measurements from varying interstation pair

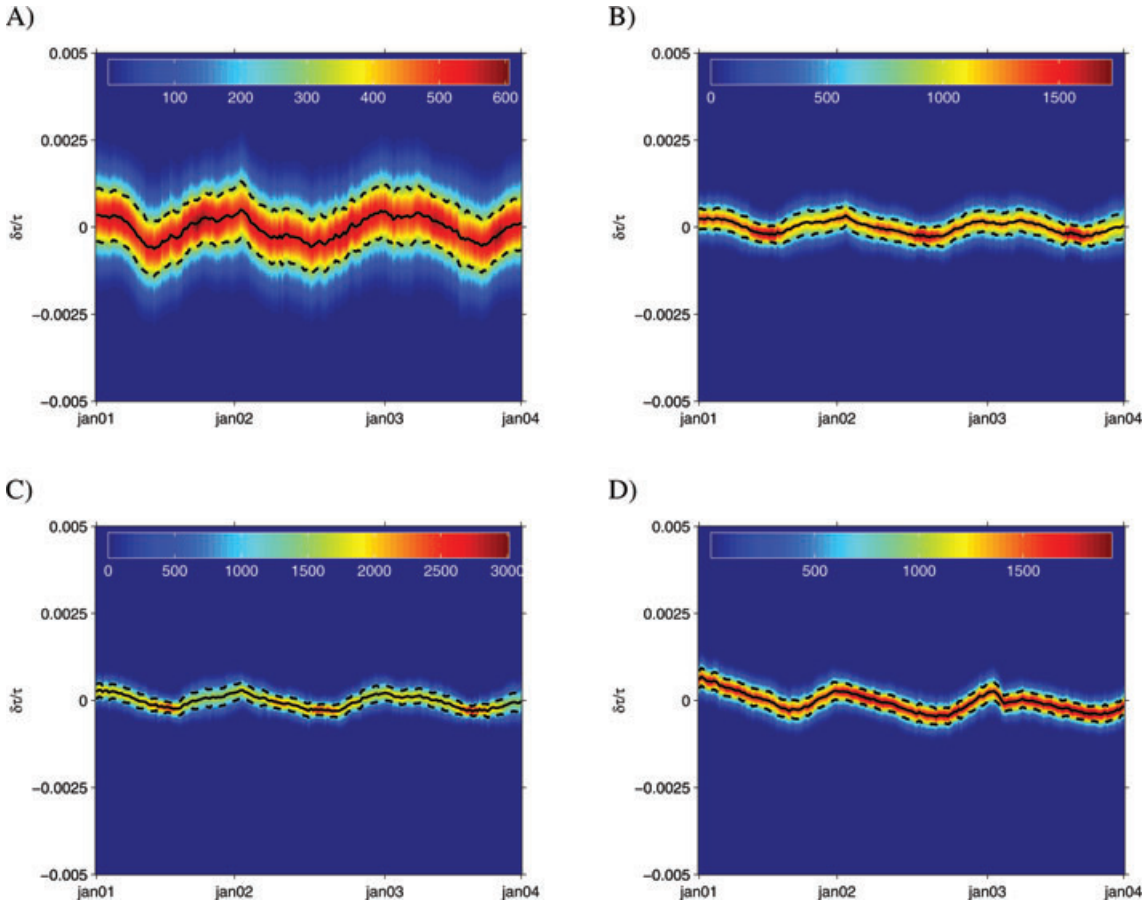

Figure 7. Gaussian pdfs of $\delta\tau/\tau$ from high quality measurements(i.e. $C_{\max} > 0.9$) with superimposed mean (black) ± 1 *SD* (dashed) for all 861 interstation pairs over a 3 yr period in various frequency bands, 0.1–0.2 (a), 0.1–1 (b), 0.1–2 (c) and 0.5–2 Hz (d).

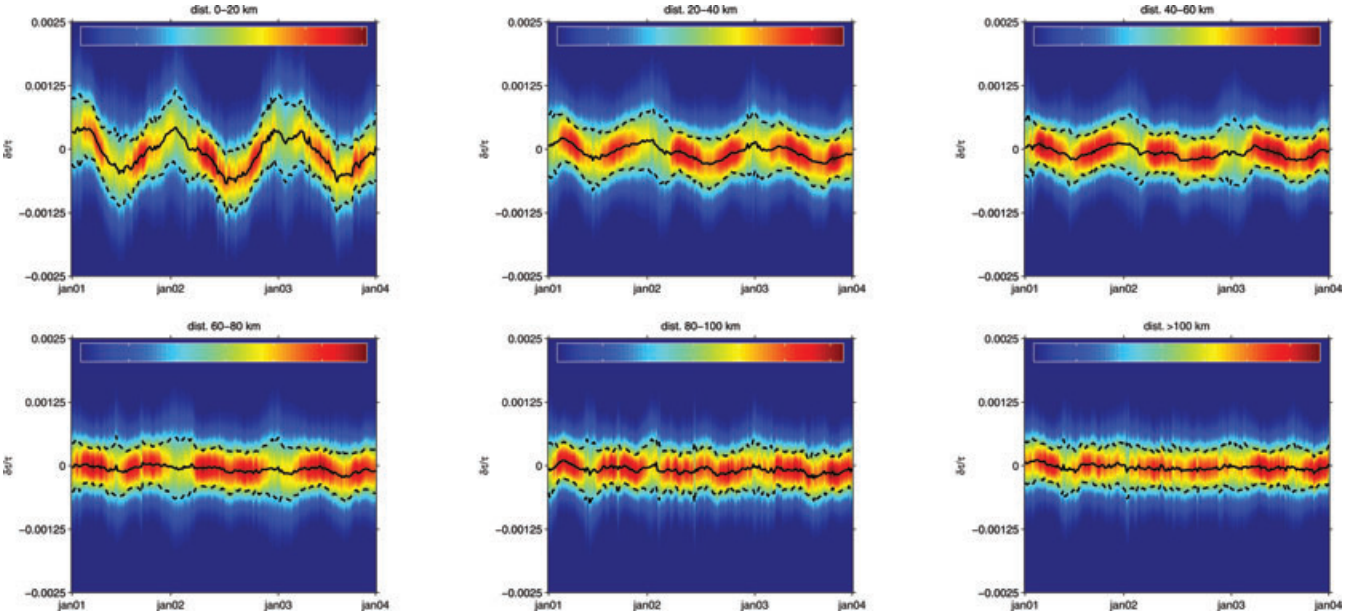

Figure 8. Gaussian pdfs of $\delta\tau/\tau$ with superimposed mean (black) ± 1 *SD* (dashed) for all 861 interstation pairs as a function of interstation pair distance in the frequency range 0.1–2 Hz.

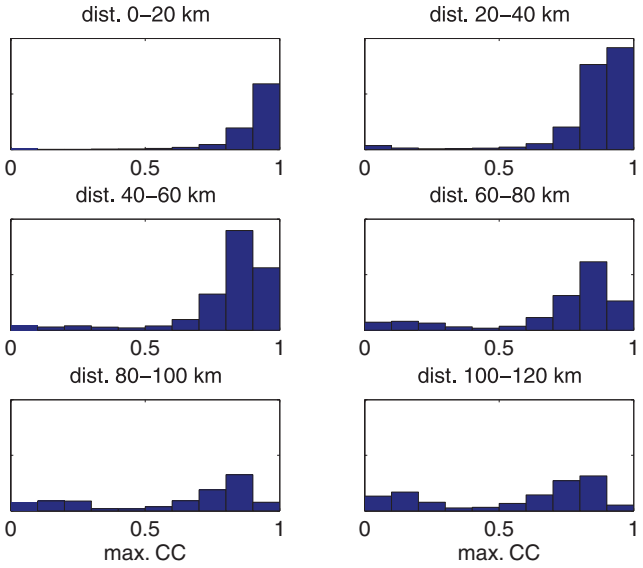

Figure 9. Histograms of the maximum correlation coefficients for all 861 interstation pairs as a function of interstation pair distance.

distances were to be combined, an adaptive way on how to choose the stacking duration would be required.

4.4 Relative time-shifts as a function of azimuth

It is well documented that the origin of seismic noise sources shows a clear seasonal variation (e.g. Stehly *et al.* 2006; Yang *et al.* 2007). In order to investigate if our observations are related to seasonal variations of the seismic sources or rather related to seasonal changes in the subsurface we investigated the dependence of $\delta\tau/\tau$ on azimuth of station pairs. If we were measuring some process related to seasonal variations of the seismic sources, that show a clear dependence on azimuth, we would expect to see the same dependence in our $\delta\tau/\tau$ measurements. In Fig. 10, $\delta\tau/\tau$ is plotted as a function of azimuth in the frequency range 0.1–2 Hz. Interestingly there seems to be no particular dependence on azimuth, for all six azimuth bins the same seasonal variations are observed. This suggests that our observations are indeed related to variations in the Earth crust and not due to seasonal variations in the noise sources.

4.5 Crude regionalization

We perform a crude regionalization by simply averaging measurements from interstation pairs that belong to three different regions. We decided to form three different clusters as indicated in Fig. 11(a). Cluster 1 (red) consists of stations in the northwestern part of the study area mainly on hard-rock sites (Fig. 11b). Cluster 2 (blue) consists of stations in the northeastern part of the study area, again mainly located on hard-rock sites (Fig. 11c). Whereas cluster 3 (green) consists of stations that are in the central part of the study area and are located within the sedimentary basin (Fig. 11d). All three clusters consist of roughly the same amount of stations and also cover a similar area. The average distributions of $\delta\tau/\tau$ of cluster 1, cluster 2 and cluster 3 are plotted in Figs 11(b), (c) and (d), respectively. Clearly the average over stations within the sedimentary basin shows the most consistent variation with a clear seasonality in $\delta\tau/\tau$. The average over stations within cluster 2 shows also a seasonal variation, but the variance is much higher and there also seem to exist additional variation over shorter time ranges. In order to further investigate if those short-term variations are simply due to instabilities in the measurements or are indeed related to processes in the upper crust a more detailed investigation would be required.

5 INTERPRETATION

As far as the interpretation of observed relative velocity changes are concerned, it is of great interest not only to monitor these changes, but also to provide an interpretation of what processes might have caused these changes. In laboratory experiments, under controlled conditions, it has been demonstrated that either changes in stress,

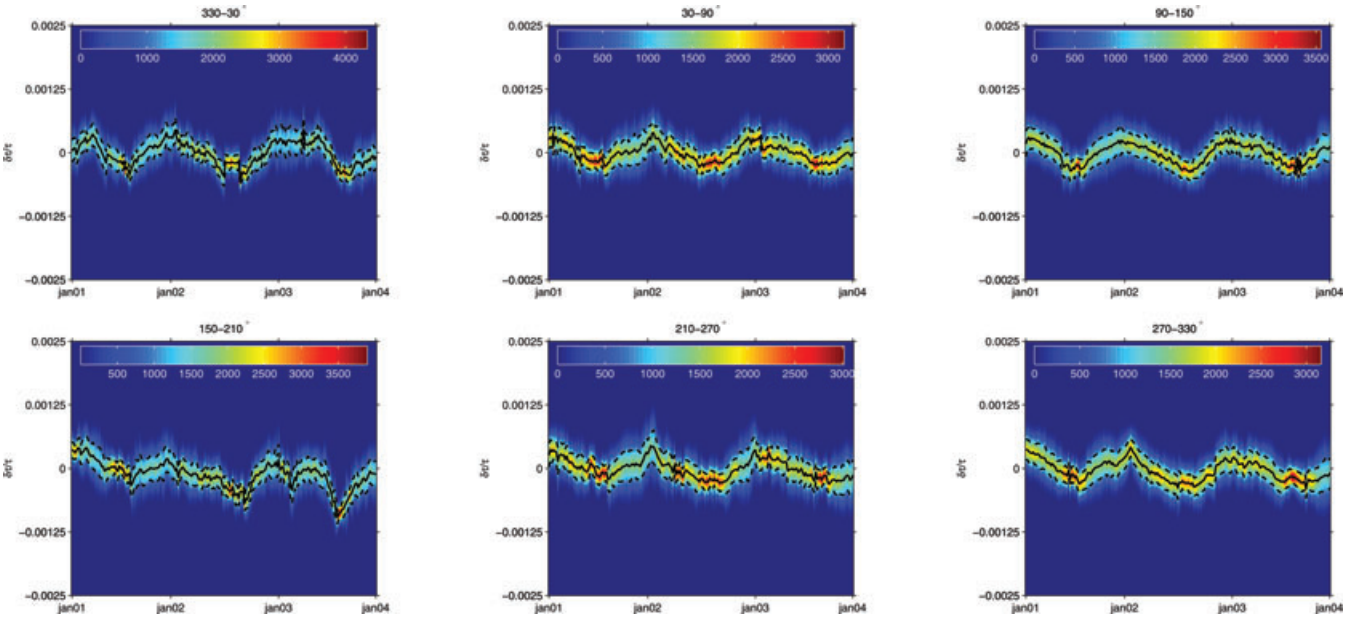

Figure 10. Gaussian pdfs of $\delta\tau/\tau$ with superimposed mean (black) ± 1 *SD* (dashed) for all 861 interstation pairs as a function of azimuth for $C_{\max} > 0.9$ in the frequency range 0.1–2 Hz.

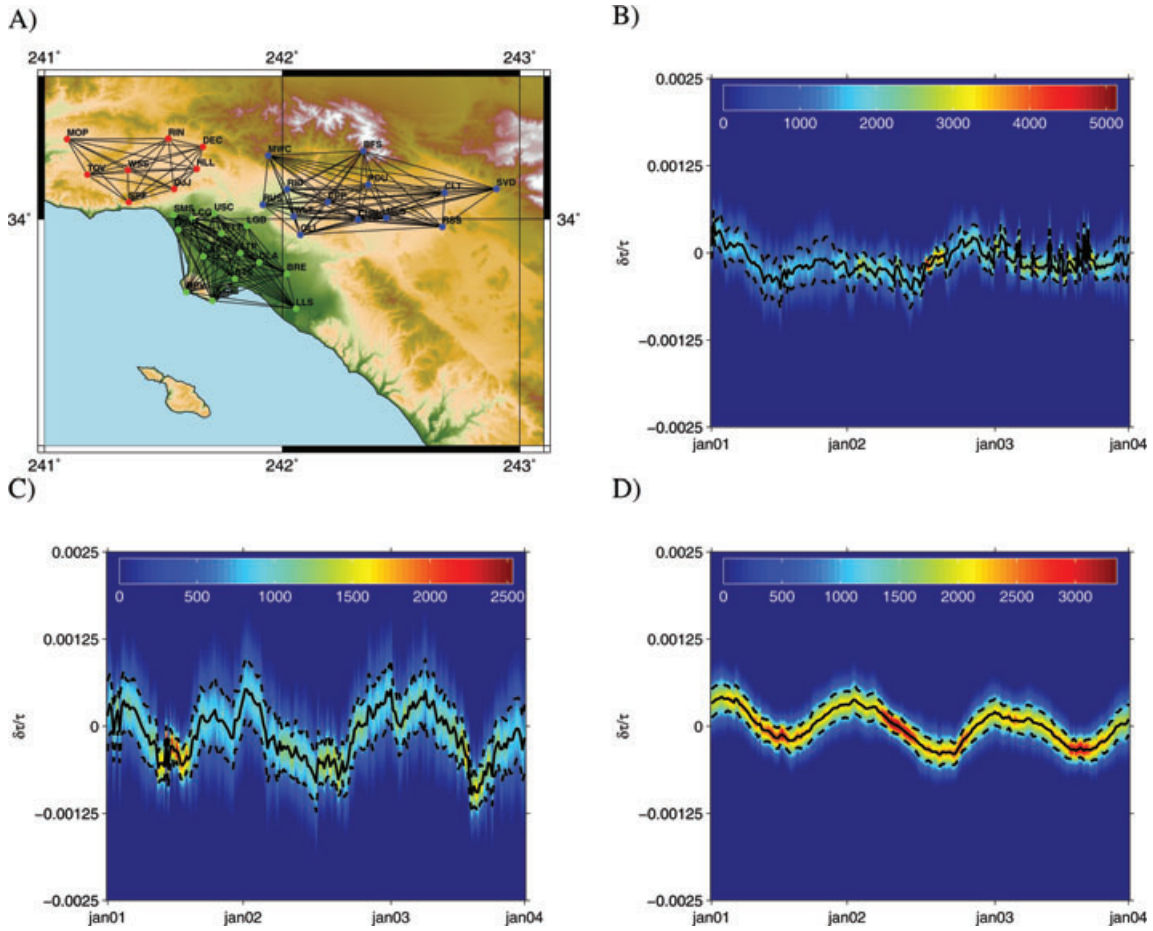

Figure 11. (a) Stations that form the three clusters whose average relative time-shifts are shown in (b) red stations, (c) blue stations and (d) green stations. Again in (b–d) Gaussian pdfs of $\delta\tau/\tau$ are shown with superimposed mean (solid) ± 1 *SD* (dashed).

temperature or water saturation result in slight velocity changes that can be detected in the coda (e.g. Weaver & Lobkis 2000; Grêt *et al.* 2006; Larose & Hall 2009). Identifying the processes that might have caused the observed velocity changes in the Earth's crust poses a more difficult problem. Recent studies presented interpretations of relative velocity changes observed at volcanoes and across the San Andreas fault (e.g. Brenguier *et al.* 2008a,b). These studies covered a rather small area and more importantly the candidate processes that might have caused the measured relative velocity changes were known beforehand (i.e. volcanic eruptions, earthquakes) and the seasonal variations were considered as background noise. Sens-Schönfelder & Wegler (2006) on the other hand observed similar seasonal variations and proposed a depth dependent hydrological model that described the seasonality in the observed relative velocity changes solely based on precipitation. This model however was based on the analysis from a single station-pair.

In the following, we discuss three different candidate processes that might have caused the observed seasonal variations within the velocity field of the Los Angeles: (1) changes in water content, (2) changes in temperature and (3) changes in stress–strain field. Seasonality of climatological variables, such as temperature, precipitation and oceanic wave height are potentially causing seasonal changes in the mechanical properties of the Earth's crust. Seasonal variations have also been observed using SAR interferometry and GPS measurements (Bawden *et al.* 2001; Watson *et al.* 2002; Argus *et al.* 2005). In these studies, observed seasonal vertical displacements have been attributed to vertical motion induced by annual variations of the groundwater table (Bawden *et al.* 2001). This hypothesis has been confirmed by Watson *et al.* (2002) who additionally analysed GPS data and found that the Los Angeles basin becomes most inflated at the beginning of the year after the rainy season when the aquifer should be at a maximum. This inflation may partially explain reduction of seismic velocities that we observe. Moreover, the observed signal is stronger within the sedimentary basin, which is also consistent with seasonal changes in hydrological parameters. At the same time, surface waves in the frequency range considered (0.1–2 Hz) are sensitive down to a depth of $\approx$10 km, which may be significantly deeper than layers affected by variations of the aquifer. Therefore, we also consider other seasonal processes such as changes in surface temperature that might affect seismic velocities in the upper crust. It has been demonstrated by Ben-Zion & Leary (1986) and more recently by Prawirodirdjo *et al.* (2006) that, while changes in surface temperature affect directly only very superficial parts of the crust, they induce thermo-elastic strain variations that persist down to a depth in the order of the surface temperature wavelength. This wavelength of the temperature field has been estimated to range from 15 to 22 km (Prawirodirdjo *et al.* 2006) in three different regions within our study area. According to Ben-Zion & Leary (1986) the amplitude of the thermo-elastic strain is over ten times larger than

the effect of ≈15 m changes of water level in a reservoir. It seems therefore more likely that the strongest variations are caused by thermo-elastically induced strain variations within the Earth's upper crust and that the seasonal variations of hydrological parameters simply further enhance these changes.

6 DISCUSSION

We computed broad-band cross-correlations from 861 interstation pairs in the Los Angeles basin and are able to monitor relative traveltime perturbations over a period of 3 yr. It is to our knowledge for the first time that these measurements have been performed for that many interstation pairs covering such a big area. On average we find a clear seasonality in the relative velocity changes. Variations between different interstation pairs have however high variance and in order to obtain stable results we had to average over close by interstation pairs. The results are therefore still rather qualitative and make a detailed interpretation difficult. A major problem we encountered is the trade-off between temporal and lateral resolution. For bigger interstation pair distances it seems that longer ambient seismic noise records have to be stacked in order to obtain meaningful measurements. An adaptive way to choose the duration over which the reference stack is built as a function of interstation pair distance might resolve some issues regarding the stability of the measurements. This would however also introduce different time-resolutions for different measurements and consequently complicate the interpretation even further.

We demonstrated how high quality measurements of relative velocity changes on a regional scale, covering an area of approximately 90×150 km, from 861 interstation pairs can be obtained. We were however only able to give an average interpretation of these measurements, averaged over three different regions. In order to provide more localized estimates of the changes in the Earth crust a better understanding of the spatial sensitivities of $\delta\tau/\tau$ measurements—ideally as a function of frequency—is required, as well as a physical model that relates traveltime perturbations to changes in material properties. This would allow us to perform a meaningful regionalization of our measurements, providing interesting insights into the dynamics of the mechanical properties of the Earth's upper crust.

ACKNOWLEDGMENTS

We thank E. Larose, P. Roux, M. Campillo and R.L. Weaver for helpful discussions, and Y. Ben-Zion for discussions regarding the thermo-elastic strain variations. UM would also like to thank M. Lambert for helpful discussions and practical advise regarding the preparation of the figures. All the data were provided by the Southern California Earthquake Data Center (SCEDC). This work was supported by an ANR contract ANR-06-CEXC-005 (COHERSIS) and an EU contract WHISPER.

REFERENCES

Argus, D.F., Heflin, M.B., Peltzer, G., Crampé, F. & Webb, F.H., 2005. Interseismic strain accumulation and anthropogenic motion in metropolitan Los Angeles, *J. geophys. Res.,* **110**(B04401), doi:10.1029/2003JB002934.

Bawden, G.W., Thatcher, W., Stein, R.S., Hudnut, K.W. & Peltzer, G., 2001. Tectonic contraction across Los Angeles after removal of groundwater pumping effects, *Nature,* **412,** 812–815.

Ben-Zion, Y. & Leary, P., 1986. Thermoelastic strain in a half-space covered by unconsolidated material, *Bull. seism. Soc. Am.,* **76,** 1447–1460.

Brenguier, F., Shapiro, N.M., Campillo, M., Nercessian, A. & Ferrazzini, V., 2007. 3-D surface wave tomography of the Piton de la Fournaise volcano using seismic noise correlations, *Geophys. Res. Lett.,* **34,** L02305, doi:10.1029/2006GL028586.

Brenguier, F., Campillo, M., Hadziioannou, C., Shapiro, N.M., Campillo, M., Nadeau, R. & Larose, E., 2008a. Postseismic Relaxation Along the San Andreas Fault at Parkfiel from Continous Seismological Observations, *Science,* **321**(5895), 1478–1481.

Brenguier, F., Shapiro, N.M., Campillo, M., Ferrazzini, V., Duputel, Z., Coutant, O. & Nercessian, A., 2008b. Towards forecasting volcanic eruptions using seismic noise, *Nature Geosience,* **126-130,** L02305, doi:10.1029/2006GL028586.

Campillo, M. & Paul, A., 2003. Long-range correlations in the diffuse seismic coda, *Science,* **299,** 547–549.

Gouédard, P. *et al.*, 2008. Cross-correlation of random fields: mathematical approach and applications, *Geophys. Prospect.,* **56,** 375–393 doi:10.1111/j.1365-2478.2007.00684.x.

Grêt, A., Snieder, R. & Scales, J., 2006. Time-lapse monitoring of rock properties with coda wave interferometry, *J. geophys. Res.,* **111**(B03305), doi:10.1029/2004JB003354.

Hadziioannou, C., Larose, E., Coutant, O., Roux, P. & Campillo, M., 2009. Stability of monitoring weak changes in multiply scattering media with ambient noise correlation: laboratory experiments, *J. acoust. Soc. Am.,* **125,** 3688–3695.

Larose, E. & Hall, S., 2009. Monitoring stress related velocity variation in concrete with a 2×10^{-5} relative resolution using diffuse ultrasound, *J. acoust. Soc. Am.,* **125,** 1853–1857.

Larose, E. et al., 2006. Correlation of random wavefields: an interdisciplinary review, *Geophysics,* **71**(4), SI11–SI21.

Leroy, V. & Derode, A., 2008. Temperature-dependent diffusing acoustic wave spectroscopy with resonant scatterers, *Phys. Rev. E,* **77,** doi:10.1103/PhysRevE.77.036602.

Lin, F.-C., Ritzwoller, M.H., Townend, J., Bannister, S. & Savage, M.K., 2007. Ambient noise rayleigh wave tomography of new zealand, *Geophys. J. Int.,* **170,** 649–666.

Moschetti, M.P., Ritzwoller, M.H. & Shapiro, N.M., 2007. Surface wave tomography of the western Unite States from ambient seismic noise: Rayleigh wave group velocity maps, *Geochem. Geophys. Geosyst.,* **8**(8), A08010, doi:10.1029/2007GC001655.

Nabney, I.T., 2002. *Netlab: Algorithms for Pattern Recognition: Advances in Pattern Recognition,* Springer Verlag, London, UK.

Nishimura, T., Uchida, N., Sato, H., Ohtake, M., Tanake, S. & Hamaguchi, H., 2000. Temporal changes of the crustal structure associated with the M6.1 earthquake on September 3, 1998 and the volcanic activity of mount Iwate, Japan, *Geophys. Res. Lett.,* **27**(2), 269–272.

Poupinet, G., Ellsworth, W.L. & Frechet, J., 1984. Monitoring velocity variations in the crust using earthquake doublets: an application to the Calaveras Fault, California, *J. geophys. Res.,* **89**(B7), 5719–5731.

Prawirodirdjo, L., Ben-Zion, Y. & Bock, Y., 2006. Observation and modeling of thermoelastic strain in Southern California Integrated GPS Network daily position time series, *J. geophys. Res.,* **111**(B02408), doi:10.1029/2005JB003716.

Sabra, K., Gerstoft, P., Roux, P., Kuperman, W. & Fehler, M., 2005a. Extracting time-domain Green's function estimates from ambient seismic noise, *Geophys. Res. Lett.,* **32**(L03310), doi:10.1029/2004GL021862.

Sabra, K., Gerstoft, P., Roux, P., Kuperman, W. & Fehler, M., 2005b. Surface wave tomography from microseisms in southern california, *Geophys. Res. Lett.,* **32**(L14311), doi:10.1029/2005GL023155.

Sens-Schönfelder, C., 2008. Synchronizing seismic networks with ambient seismic noise, *Geophys. J. Int.,* **174,** 966–970.

Sens-Schönfelder, C. & Wegler, U., 2006. Passive image interferometry and seasonal variations of seismic velocities at Merapi Volcano, Indonesia, *Geophys. Res. Lett.,* **33,** L21302, doi:10.1029/2006GL027797.

Shapiro, N.M. & Campillo, M., 2004. Emergence of broadband Rayleigh waves from correlations of the ambient seismic noise, *Geophys. Res. Lett.,* **31,** doi:10.1029/2004GL019491.

Shapiro, N.M., Campillo, M., Stehly, L. & Ritzwoller, M.H., 2005. High-resolution surface-wave tomography from ambient seismic noise, *Science,* **307,** 1615–1617.

Snieder, R., Grêt, A., Douma, H. & Scales, J., 2002. Coda wave interferometry for estimating nonlinear behaviour in seismic velocity, *Science,* **295,** 2253–2255.

Stehly, L., Campillo, M. & Shapiro, N.M., 2006. A study of the seismic noise from its long-range correlation properties, *J. geophys. Res.,* **111**(B10306), doi:10.1029/2005JB004237.

Stehly, L., Campillo, M. & Shapiro, N.M., 2007. Traveltime measurements from noise correlation: stability and detection of instrumental time-shifts, *Geophys. J. Int.,* **171,** 223–230.

Stehly, L., Fry, B., Campillo, M., Shapiro, N.M., Guilbert, J., Boschi, L. & Giardini, D., 2009. Tomography of the alpine region from observations of seismic ambient noise, *Geophys. J. Int.,* **178,** 338–350.

Watson, K.M., Bock, Y. & Sandwell, D.T., 2002. Satellite interferometric observations of displacements associated with seasonal groundwater in the Los Angeles basin, *J. geophys. Res.,* **107**(B4), 2074, doi:10.1029/2001JB000470.

Weaver, R.L. & Lobkis, O., 2000. Temperature dependence of diffuse field phase, *Ultrasonics,* **38,** 491–494.

Weaver, R.L. & Lobkis, O., 2001. On the emergence of the Green's function in the correlations of a diffuse field, *J. acoust. Soc. Am.,* **110,** 3011–3017.

Wegler, U. & Sens-Schönfelder, C., 2007. Fault zone monitoring with passive image interferometry, *Geophys. J. Int.,* **168,** 1029–1033.

Wegler, U., Lühr, B.-G., Snieder, R. & Ratdomopurbo, A., 2006. Increase of shear wave velocity before the 1998 eruption of Merapi volcano (Indonesia), *Geophys. Res. Lett.,* **33,** L09303, doi:10.1029/2006GL025928.

Yang, Y., Ritzwoller, M.H., Levshin, A.L. & Shapiro, N.M., 2007. Ambient noise Rayleigh wave tomography across Europe, *Geophys. J. Int.,* **168,** 259–274.